



Precision measurements of the zero-temperature dielectric constant and density of liquid ^4He

R. T. Learn , E. Varga ,* V. Vadakkumbatt , and J. P. Davis [†]

Department of Physics, University of Alberta, Edmonton, Alberta, Canada T6G 2E1



(Received 27 June 2022; revised 20 October 2022; accepted 28 November 2022; published 12 December 2022)

The resonant frequencies of three-dimensional (3D) microwave cavities are explicitly dependent on the dielectric constant of the material filling the cavity, making them an ideal system for probing material properties. In particular, dielectric constant measurements allow one to extract the helium density through the Clausius-Mossotti relation. By filling a cylindrical aluminum cavity with superfluid helium, we make precision measurements of the dielectric constant of liquid ^4He at saturated vapor pressure for range of temperatures 30 to 300 mK and at pressures of 0 to 25.0 bar at 30 mK, essentially the zero temperature limit for the properties of ^4He . After reviewing previous measurements, we find systematic discrepancy between the low and high frequency determination of the dielectric constant in the zero-temperature limit and moderate discrepancy with previously reported values of pressure-dependent density. Our precision measurements suggest 3D microwave cavities are a promising choice for refining previously measured values in helium, with potential applications in metrology.

DOI: [10.1103/PhysRevB.106.214509](https://doi.org/10.1103/PhysRevB.106.214509)

I. INTRODUCTION

Three-dimensional (3D) microwave cavities are an important tool for the physicist. For example, they are used as accelerating cavities in particle colliders [1] and are often used in combination with transmon qubits [2,3]—one of the most promising qubit architectures. One reason for the ubiquity of the 3D microwave cavity is that the open structure allows the electric and magnetic fields to reside in a material-free volume, reducing dissipation from lossy materials [4,5]. This can be compared with on-chip microwave cavities, where substrate loss from two-level systems [6–8] generally dominates. Furthermore, the open structure allows for the incorporation of materials into the microwave cavity [9,10] making 3D cavities a valuable tool for precision measurements of material properties [11,12].

Incorporating superfluid ^4He with microwave systems is beneficial for multiple applications. Filling a 3D microwave cavity with superfluid helium allows easy tunability of the cavity frequency [13], and improves thermalization of superconducting qubits [14]; superfluid helium, when coupled to a microwave optomechanical system, is a promising mechanical medium for proposed detectors of gravitational waves [15–18] and dark matter [19]. It also allows novel studies of two-dimensional (2D) electron systems [20], including the design of a new type of qubit [21].

Here, we use a 3D microwave cavity for a precision study of the dielectric constant and density of superfluid ^4He in the low-temperature limit. Using the Clausius-Mossotti relation, the dielectric constant measurements can be interpreted as measurements of the helium density, in a manner essentially similar to approaches such as dielectric constant (or refractive

index) gas thermometry [22,23]. The ability to resolve small frequency shifts in the high- Q microwave cavity allows this to be done with precision comparable to—or exceeding—the state-of-the-art capacitance measurements [8,24–29]. Interestingly, for the temperature dependence of the dielectric constant, we find a systematic discrepancy between low (capacitive) and high (microwave resonance) frequency determination of the dielectric constant, which cannot be accounted for by frequency dependence of the polarizability. For a particular choice of polarizability of helium [23], we find good agreement with the commonly used literature values [30,31] of pressure dependence of the low-temperature density and the speed of sound. We find the largest sources of uncertainty to originate in the value of the molar polarizability of liquid helium and complex deformation of the cavity in a pressurized bath.

II. THEORY

The helium density was calculated by measuring the resonant frequency of a cylindrical microwave cavity, which will have standing-wave modes determined by Maxwell's equations. For a right cylinder with height h and radius a , the resonant frequencies for transverse electric (TE) modes, where $E_z = 0$ with z the axis of the cylinder, are given by [32]

$$f_{nm} = \frac{c}{2\pi\sqrt{\mu_r\epsilon_r}} \sqrt{\left(\frac{x'_{nm}}{a}\right)^2 + \left(\frac{l\pi}{h}\right)^2}, \quad (1)$$

where x'_{nm} is the m th zero of the derivative of the n th Bessel function of the first kind, c is the speed of light, and μ_r , ϵ_r are the relative permeability and permittivity, respectively, of the material filling the cavity. In particular, we are interested in the TE_{011} and TE_{111} modes, pictured in Fig. 1. Particularly for the mode TE_{011} , since the electric field vanishes at all surfaces for this mode, dielectric and seam losses are negligible

*emil.varga@matfyz.cuni.cz

[†]jdavis@ualberta.ca

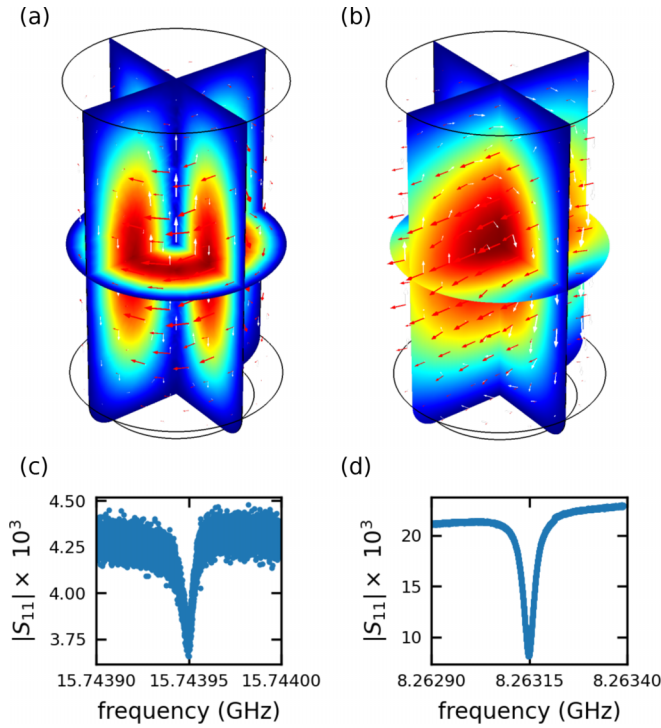


FIG. 1. (a) Finite-element simulation of the electric field for the TE_{011} mode of a right cylindrical cavity with resonance frequency 15.693 GHz at room temperature. Red arrows show the direction of electric field, while white arrows show the direction of magnetic field. The lower edge of the cavity is filleted to split the desired TE_{011} mode from the low- Q degenerate TM_{111} mode. (b) Simulation of the electric field for the TE_{111} mode. (c) Example measurement for the TE_{011} mode while in-vacuum at base temperature, with a total Q of 2×10^6 . (d) Example measurement for the TE_{111} mode while in-vacuum at base temperature, with a total Q of 1.6×10^5 .

and only conductor losses contribute [33]. This results in a low loss rate and hence a high-quality mode capable of achieving internal quality factors on the order of 10^8 for high-purity aluminum cavities [4].

When filling a microwave cavity with superfluid helium, only the relative permittivity of the material inside the cavity changes, and the filled resonant frequency f_{filled} will be reduced from the in-vacuum resonant frequency f_{empty} by the relation

$$f_{\text{filled}} = \frac{f_{\text{empty}}}{\sqrt{\epsilon_{\text{He}}}}, \quad (2)$$

where ϵ_{He} is the dielectric constant of superfluid ^4He . This allows us to directly calculate the dielectric constant by comparing measurements of the filled and in-vacuum resonant frequencies as

$$\epsilon_{\text{He}} = \left(\frac{f_{\text{empty}}}{f_{\text{filled}}(P)} \right)^2. \quad (3)$$

This expression, however, needs to be corrected for finite compressibility of the cavity walls [see Eq. (10) below].

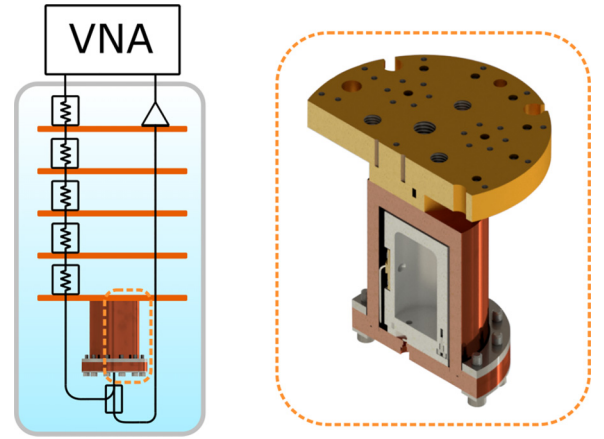


FIG. 2. (a) Diagram of the circuit used to take measurements. A total of 34 dB of attenuation reduces the signal from the VNA before reaching the cavity, including the directional coupler which transmits and receives the S_{11} signal. A low-noise HEMT amplifies the signal at the 4 K stage before returning to the VNA. (b) Cross-section of the experimental apparatus used to measure the dielectric constant of helium-4. The microwave cavity is placed inside a hermetically sealed cell, which is then filled with helium, preventing pressure differentials across cavity walls.

The dielectric constant and density are related through the Clausius-Mossotti relation

$$\frac{\epsilon_{\text{He}} - 1}{\epsilon_{\text{He}} + 2} = \frac{4\pi}{3} \frac{\alpha}{M} \rho, \quad (4)$$

where α is the polarizability volume per mole (shortened to “polarizability” henceforth), M is the molar mass of ^4He , and ρ is the density [34].

Finally, given a pressure dependence of the density, the long-wavelength limit of the speed of sound is

$$c = \left(\frac{\partial \rho}{\partial p} \right)^{-1/2}. \quad (5)$$

III. EXPERIMENTAL SETUP

The dielectric constant was measured using a superconducting cylindrical aluminum microwave cavity cooled to approximately 30 mK using a dilution refrigerator, as schematically shown in Fig. 2. The cavity was machined to be 2.4 cm in diameter and 4-cm tall at room temperature for an approximate total volume of 18 cm^3 . The cavity was designed to operate in the TE_{011} and TE_{111} modes, with measured resonant frequencies of 15.74 GHz and 8.26 GHz, respectively, for $T = 30 \text{ mK}$. For our cavity machined out of 6061 aluminum, we measured an internal quality factor at 30 mK of $\sim 2 \times 10^6$ for TE_{011} . Higher quality factors could be achieved with pure aluminum or niobium [4,35]. The TE_{011} mode of a perfectly cylindrical cavity is degenerate with the low- Q TM_{111} mode. To break this degeneracy, a 1-inch-radius fillet was added to the bottom edge of the cavity. The microwave cavity was placed inside a hermetically sealed copper cell, as shown in Fig. 2(b). This design allows helium to freely flow in and around the microwave cavity such that there are no pressure differentials across the walls of the cavity. This eliminates the

possibility of the cavity bowing under high pressures, which can shift the resonant frequency of the cavity considerably, as was seen in past measurements [13].

The complex-valued reflection from the cavity is fit to the expected frequency dependence of the scattering parameter [36]

$$S_{11}(f) = Ae^{i(f\tau + \phi_0)} \left(1 - \frac{2e^{i\phi_Z} \frac{Q_{\text{tot}}}{Q_{\text{ext}}}}{1 + 2iQ_{\text{tot}} \left(\frac{f}{f_0} - 1 \right)} \right), \quad (6)$$

where f_0 is the resonance frequency, ϕ_Z characterizes impedance mismatch, and A , τ , and ϕ_0 characterize the overall loss, delay, and phase rotation due to wiring and amplification within the cryostat [36]. The total quality factor is given by $Q_{\text{tot}}^{-1} = Q_{\text{ext}}^{-1} + Q_{\text{int}}^{-1}$ where Q_{ext} is the external quality factor characterizing the coupling to the microwave mode and Q_{int} is the internal quality factor due to all other dissipation processes [36].

The cavity was coupled to using a pin coupler, which was aligned parallel to the electric field of the TE_{011} mode. By adjusting the length of the pin coupler, we decreased the coupling such that the external quality factor was $\sim 3 \times 10^7$ at base temperature. This meant that the total cavity quality factor was almost entirely limited by internal losses, allowing for maximum precision in our measurements.

To take measurements in the zero-temperature limit, the cell was mounted on the mixing chamber plate of a dilution refrigerator. The resonant modes were measured using a vector network analyzer (VNA) in an RF circuit shown in Fig. 2(a). At each stage of the dilution refrigerator, attenuators were used to heat sink the microwave coaxial line, attenuating the signal a total of 24 dBm. A directional coupler with 10 dB of attenuation was used to transmit the microwave power to and from the cavity. The reflected signal was then amplified through a low noise amplifier at the 4 K stage of the refrigerator and returned to the VNA.

The temperature of the mixing chamber was measured using an ultra-low-temperature ruthenium oxide sensor and controlled through an AC resistance bridge. Close to the base temperature, we were able to achieve temperature stability of 0.5 mK, while at higher temperatures ($T \approx 300$ mK) temperature stability decreased to 1 mK. The pressure of the helium inside the cell was set using a homemade control system, which consists of a ballast volume immersed in liquid nitrogen with a resistive heater controlled by a proportional–integral–derivative (PID) loop. The stability of the pressure measured at room temperature was about 1 mbar.

The data were measured during two separate cool downs of the dilution refrigerator separated by few a months. These data sets will be referred to as Run 1 and Run 2. Once at base temperature ($T \approx 30$ mK), measurements of both TE_{011} and TE_{111} modes were taken in a vacuum over several days to ensure that the resonant frequency was stable. The resonant frequency was observed to shift no more than a few hundred Hz (i.e., less than 1 ppm), which is within the precision of the fitting method used. Before filling the cavity with liquid helium, the temperature dependence of the microwave modes was measured in the range 30 to 300 mK. The cavity was then filled with helium by condensing He gas from a commercial high-pressure cylinder through a sintered copper heat

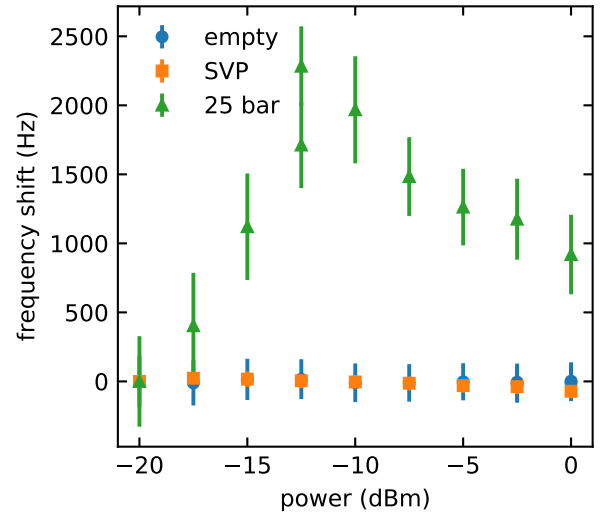


FIG. 3. The shift in frequency of the TE_{011} mode as the power (at source) is decreased from 0 to -20 dBm, for three separate sets of measurements: in-vacuum (blue), filled with helium at saturated vapor pressure (orange), and pressurized to 25 bar (green). The zero-point is taken as the -20 dBm for each respective dataset.

exchanger placed on 4 K, 1 K, still (approximately 0.8 K), and mixing chamber stages of the dilution refrigerator. Measurements were taken first at saturated vapor pressure (SVP, only for Run 2) again in the temperature range 30 to 300 mK. Finally, the cell was pressurized up to 25 bar in approximately 0.5 bar steps. For each pressure or temperature, 200 traces of the S_{11} signal were taken in relatively quick succession (entire acquisition taking several minutes) for both modes, which were individually fit using Eq. (6) to find the resonant frequency and its standard deviation.

IV. DRIVE POWER ANALYSIS

To ensure that the drive power would not heat the cavity, the effect of the VNA drive power was measured for the cavity while in-vacuum, filled to SVP, and pressurized to 25.0 bar. In each set of measurements, the drive power at source was varied from -20 to 0 dBm (0.01 to 1.00 mW), and the resonant frequency of the TE_{011} mode was measured.

Figure 3 shows the resonant frequency of the TE_{011} mode for powers between 0 and -20 dBm while in-vacuum, filled to SVP, and pressurized to 25 bar. Heating of the cavity ought to correspond to decrease of the resonance frequency [33], which is observed weakly for the empty and SVP data. The origin of the peak in frequency shift for the 25 bar data is unknown, but it is unlikely to be related to the heating of the cavity itself. Nevertheless, even at the peak, the relative frequency shift is small and we use -10 dBm drive power which we find to be a good compromise between low-pressure heating and signal-to-noise ratio. However, to account for power-dependent frequency shifts we include an additional 100 Hz error on resonance frequencies measured at saturated vapor pressure (the data in Sec. VI A) and additional 2500 Hz error on all resonance frequencies measured at increased pressures (the data in Sec. VI B).

V. CORRECTIONS DUE TO SYSTEMATIC ERRORS

The low-temperature density of ^4He was measured in the range 0.5 to 25.0 bar. While at 30 mK, the cell was pressurized in steps of 1 bar. Measurements were taken while ramping up the pressure from 1.0 to 25.0 bar, and then ramping down the pressure from 24.5 to 0.5 bar. There are multiple known sources of systematic error related to the pressure that may affect our measurements. Here we identify and correct for the following: (1) a hydrostatic pressure head; (2) superfluid fountain pressure; and (3) compression of the aluminum cavity.

(1) A hydrostatic pressure head arises from excess liquid helium in the fill line a height h above the microwave cavity. This will not affect the measured frequency, but will shift the pressure in the cell P_{cell} from what is measured at room temperature P_{meas} to

$$P_{\text{cell}} = P_{\text{meas}} + \rho gh, \quad (7)$$

where g is the acceleration due to gravity.

Since the level of helium in the dewar surrounding the dilution unit is not constant, the level of liquid helium in the cell fill line will fluctuate, changing the hydrostatic pressure head. We estimate that the liquid level will vary between 59 and 79 cm above the cavity. We correct our data for a hydrostatic pressure head of height $h = 68.5$ cm, but consider the 59 to 79 cm range as one component of the uncertainty of the pressure reading.

(2) When two reservoirs of He-II at different temperatures are connected via a thin channel that does not admit the flow of the viscous normal fluid component, a pressure difference develops according to

$$\nabla p = \rho S \nabla T, \quad (8)$$

where S is the specific entropy [37]. The helium fill line of the cell passes through sintered copper heat exchangers on each stage of the dilution refrigerator that strongly restrict the flow of helium. Assuming that the effect is negligible below the temperature of the still ($T_{\text{still}} \approx 0.8$ K) we assume that the pressure drop is dominated by the temperature gradient across the heat exchanger at the 1 K pot ($T_{\text{pot}} \approx 1.45$ K), i.e.,

$$\Delta p_{\text{fountain}} = \int_{T_{\text{still}}}^{T_{\text{pot}}} \rho(p, T) S(p, T) dT, \quad (9)$$

which has to be subtracted from the pressure measured at room temperature to obtain the correct cell pressure. We also assume that the hydrostatic and fountain pressure are balanced and helium is stationary (and thus we neglect interaction with remnant pinned vortices). Here, for $\rho(p, T)$ and $S(p, T)$, the HEPAK dataset was used [38] and the influence of the pressure gradient on the material parameters ρ and S was neglected. The resulting fountain pressure correction is shown in Fig. 4.

(3) As the pressure of the helium increases, the cavity frequency will also be affected by deformation of the cavity itself. We correct for the deformation of the cavity using the procedure found in Ref. [12]: assuming small elastic deformation, all cavity dimensions d (i.e., radius a and height h) will be renormalized to $d = d_0(1 - P/3K)$ where P is the pressure, K the bulk modulus of the cavity material, and d_0 is the cavity dimension at $P = 0$. The dielectric constant corrected

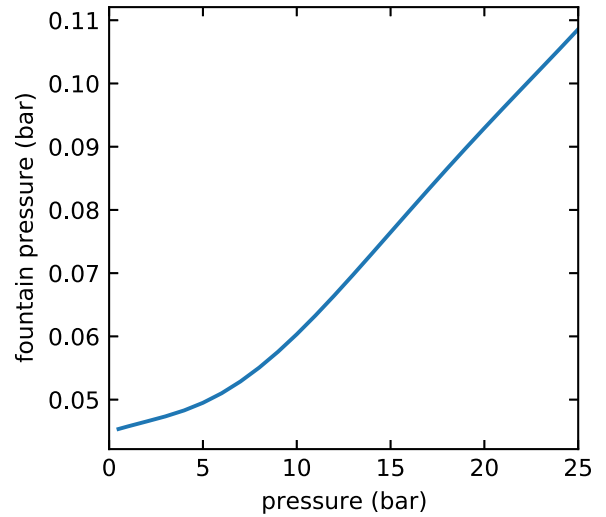


FIG. 4. Pressure difference between two ends of a superleak due to the fountain effect calculated using (9). End temperatures are assumed to be 0.8 K and 1.45 K.

for deformation is thus [cf. Eq. (1)]

$$\varepsilon_{\text{He}} = \left(\frac{f_{\text{empty}}}{f_{\text{filled}}(P)} \right)^2 \frac{1}{(1 - P/3K)^2}. \quad (10)$$

The bulk modulus is related to the Young's modulus E through $K = E/3(1 - 2\nu)$, where for Al the Poisson ratio $\nu = 0.33 \pm 0.01$. The value of the Young's modulus E of Al alloy 6061 at low temperatures reported in the literature varies in the range [39,40] 77.7 to 78 GPa. Error estimates are generally not available. Conservatively, we chose $E = 77.8 \pm 0.5$ GPa. The uncertainties of pressure, E , and ν are propagated into the uncertainties ε shown below. The yield stress of 6061 is in the range of 350 MPa [39], making corrections due to plastic deformation under our highest applied pressure, approximately 2.5 MPa, negligible.

Finally, a significant source of uncertainty for calculating the density from the measured frequency shift and dielectric constant using Eq. (4) is the value of the polarizability α of liquid ^4He . Various values for the molar polarizability were obtained [12,26,38,41,42], which disagree on the level of about 0.1%. Indeed, even the existence of the temperature dependence of polarizability at fixed pressure is uncertain, with the authors of Refs. [12,43] giving contradicting results. For helium in the gas phase, the value of the polarizability is known to satisfactory precision with ppm-level agreement between experiment [23] and *ab initio* theory [44]. However, due to interatomic interactions, the Clausius-Mossotti equation requires a virial expansion [45,46], suggesting that the value of the effective polarizability of the liquid used in Eq. (4) will likely differ from the polarizability of individual atoms [47,48].

Despite these difficulties, we believe the currently available low-density value of polarizability is the most reliable. In the following, we calculate the density and speed of sound using the polarizability measured with a dielectric constant gas thermometer near the triple point of water [23], which produces the best absolute agreement with previously accepted

values of density [30,31] without the necessity of explicitly correcting using an external reference [29].

VI. RESULTS

A. Temperature dependence of the dielectric constant at saturated vapor pressure

The temperature dependence of the dielectric constant was measured in the past, but few have measured it in the low-temperature limit. Chan *et al.* [43] measured the dielectric constant using a parallel plate capacitor in the range 100 to 1200 mK. They obtained their value for the dielectric constant at zero temperature ϵ_0 by extrapolating their data using

$$\epsilon_{\text{He}} = \epsilon_0 + (\epsilon_0 - 1)(A_4 T^4 + A_6 T^6), \quad (11)$$

which they fit for temperatures up to 300 mK with fixed $A_4 = -(2.9 \pm 0.01) \times 10^{-4} \text{ K}^{-4}$ based on the speed-of-sound measurements found in Ref. [31]. Only Berthold *et al.* [12] directly measured the dielectric constant at SVP in the low-temperature limit. Their method was similar to ours—they measured the resonant frequency of the TE_{011} mode of a cylindrical niobium cavity at 91 mK. The most recent measurement of the dielectric constant was made by Niemela and Donnelly [28] who only measured the dielectric constant above 1 K, but extrapolated to zero temperature using empirical formulas.

We measured the dielectric constant at saturated vapor pressure (SVP) during Run 2 using the TE_{011} mode. This was done by slowly filling the cell while watching the frequency shift using the VNA. Once the frequency stabilized, the cell was assumed to be filled, and the filling was halted by closing a room-temperature valve in the gas handling system. This method leads to some uncertainty in the height of the helium above the cell, which would increase the pressure in the cell from SVP by an unknown amount. Assuming the pressure head is no more than 1 cm above the cavity, the pressure would be increased by, at most, 10^{-4} bar. The temperature was increased in steps of 25 mK from 30 to 330 mK, and the shift in the resonant frequency was measured. These data were then compared to in-vacuum data at the same temperature through Eq. (2). The temperature dependence of mode TE_{111} shows a much larger scatter than TE_{011} , probably due to increased sensitivity of the mode inner surface of the cavity [12] and thus to the position of the pin coupler, which is susceptible to motion due to pressure fluctuations and mechanical vibrations.

Figure 5 plots our calculated dielectric constant at SVP as a function of temperature. Following Chan [43], we fit our data to Eq. (11) with $A_4 = -(2.9 \pm 0.01) \times 10^{-4} \text{ K}^{-4}$ fixed (orange dashed line in Fig. 5), finding the zero-temperature dielectric constant ϵ_0 and the fitting parameter A_6 to be

$$\epsilon_0 = 1.05727756 \pm 2 \times 10^{-8},$$

$$A_6 = (9 \pm 5) \times 10^{-6} \text{ K}^{-6}.$$

The uncertainties were estimated using a Monte Carlo method, where multiple datasets were generated by drawing a random sample for each temperature from a normal distribution centered on the experimental mean and with variance equal to the square of the experimental error estimate. Each generated dataset was fit using Eq. (11); the values shown

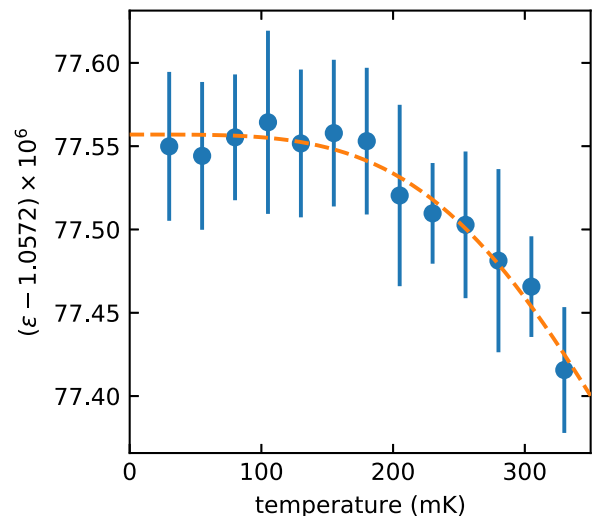


FIG. 5. The dielectric constant of helium at saturated vapor pressure for temperatures between 30–330 mK measured using the TE_{011} mode and calculated using (2). The error bars were calculated using the statistical errors on f_{filled} and f_{empty} , which were obtained by measuring the cavity resonance 200 times. The dashed line is a fit to temperature dependence given by (11). For the dielectric constant obtained using the TE_{111} mode (not shown), the temperature dependence was obscured by increased scatter but is consistent with TE_{011} within approximately 3 ppm.

above are the averages and standard deviations of a set of the individual fit parameters. The procedure was repeated for a sufficiently high number of samples such that the estimates of values and their error converged. The large uncertainty on A_6 is due to weak temperature dependence of ϵ in the range accessible to the present experiment, which results in a poorly conditioned fit.

Another source of uncertainty not captured in the statistical analysis outlined above is due to imperfect realization of the saturated vapor pressure due to the unknown hydrostatic head. Based on the measured pressure dependence [see Eq. (12) below] we can estimate the slope $\epsilon' = d\epsilon/dP = (7 \pm 4) \times 10^{-4} \text{ bar}^{-1}$. Estimating the hydrostatic pressure uncertainty based on the cell height $h = 4$ cm as $\delta P = \rho gh \approx 0.6$ mbar, which yields additional error on the dielectric constant $\delta_P \epsilon = \epsilon' \delta P \approx 4 \times 10^{-7}$, which dominates the total uncertainty.

It should be stressed that the uncertainties reported here for the SVP data are obtained only for a single experimental run. Additional mechanisms, not characterized in the present experiment, can potentially increase the actual uncertainty of the low-temperature dielectric constant. These could include, for example, irreversible deformation of the cavity during the cooling and warming cycles, or the variable isotopic purity of helium. At increased pressure (see below) we observe the reproducibility of the dielectric constant to within about 10 ppm between Run 1 and Run 2, although this is likely dominated by deformation of the cell at high pressure and should be significantly less at SVP.

Table I summarizes the values for the zero-temperature dielectric constant obtained by several studies. Chan *et al.* [43] extrapolated the high-temperature data of Kierstead [42] and Harris-Lowe and Smee [26] to obtain a zero-temperature

TABLE I. Various values for the dielectric constant of ^4He at saturated vapor pressure extrapolated to $T = 0$. The column “method” shows whether the experiment measured a capacitance change of a helium-filled capacitor or a shift of resonant frequency of a microwave cavity (as in the present experiment). The error in our result includes the error due to imperfect realization of the SVP.

Authors	Method	ϵ_0
Niemela and Donnelly [28]	Capacitance	1.057255
Chan <i>et al.</i> [43]	Capacitance	1.0572190(5)
Kierstead [42] ^a	Capacitance	1.0571374(10)
Harris-Lowe and Smee [26] ^a	Capacitance	1.0572467(100)
Tanaka <i>et al.</i> [29]	Capacitance	1.0572025
Berthold <i>et al.</i> [12]	Cavity	1.0572784(5)
Current authors	Cavity	1.0572776(4)

^aExtrapolated to zero-temperature by Chan *et al.*

value. Note in Table I that the value of the zero-temperature dielectric constant obtained here is systematically higher, and outside of the estimated error bars, than previously reported values measured using helium-filled capacitors, but in relatively good agreement with Ref. [12], the only other work measured using a microwave cavity. The reason for this relatively large and apparently systematic discrepancy between low-frequency and high-frequency estimation of the dielectric constant is, at present, unknown since the relative change in polarizability between DC and 15 GHz is expected to be negligible, on the order of 10^{-12} [44].

B. Pressure dependence of dielectric constant and density

The corrected results for the low-temperature pressure-dependent dielectric constant are shown in Fig. 6. This includes data taken over two separate runs, using two different microwave modes, increasing and decreasing pressure ramp, and a separate measurement at saturated vapor pressure.

Since the calculation of the density from the dielectric constant depends on polarizability, which is not presently known with sufficient accuracy for liquid helium, we adopt an approach common in dielectric constant gas thermometry [23] and fit the pressure dependence of the Clausius-Mossotti parameter $\mu = (\epsilon - 1)/(\epsilon + 2) \propto \rho$ (the proportionality assumes that the polarizability is density-independent) using a third degree polynomial

$$P = A_0 + A_1\mu + A_2\mu^2 + A_3\mu^3, \quad (12)$$

where A_n are fit parameters. To account for measurement errors in both pressure and dielectric constant, Eq. (12) was fit to the data using orthogonal distance regression (ODR) weighted by the estimated uncertainties of the individual measurements of pressure and μ [49]. The errors of the fit parameters were estimated by the ODR fitting routines and checked by bootstrapping [50]. The resulting parameter values are

$$A_0 = -105 \pm 7\text{bar},$$

$$A_1 = (2.0 \pm 0.1) \times 10^4\text{bar},$$

$$A_2 = (-1.46 \pm 0.05) \times 10^6\text{bar},$$

$$A_3 = (3.72 \pm 0.08) \times 10^7\text{bar}.$$

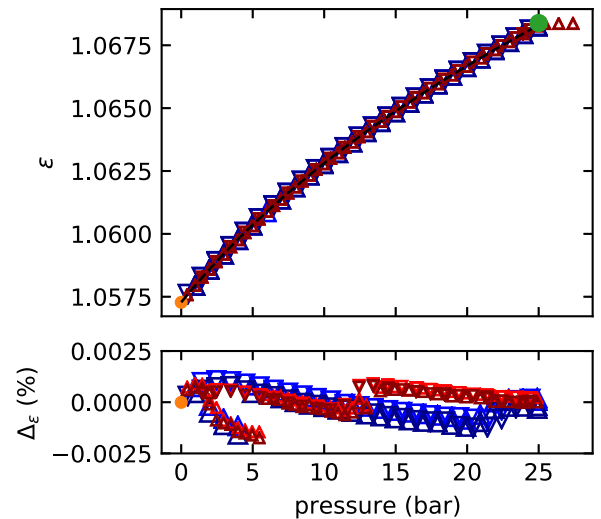


FIG. 6. Pressure dependence of the dielectric constant (top) and the residuals from the fit (12) (bottom). The data above 25 bar, where helium solidifies, were excluded from the fit. Up-triangles correspond to increasing pressure ramp, down-triangles to decreasing pressure; smaller red points to run 1 and larger blue points to run 2; lighter colors to mode TE_{011} and darker colors to TE_{111} . The full orange circle shows the dielectric constant at the saturated vapor pressure. The full green circle shows the freezing-point dielectric constant of Berthold *et al.* [12].

To invert Eq. (12) and obtain the $\mu(P)$ [and $\epsilon(P)$] relationship a standard root-finding algorithm is employed. The relative residuals $\Delta_\epsilon = (\epsilon - \epsilon_{\text{fit}})/\epsilon_{\text{fit}}$ are shown in the bottom panel of Fig. 6. In the plot of the residuals, there are two distinct jumps in the data. The first jump occurs in both runs at $P \sim 5$ bar while increasing the pressure, but does not follow the same behavior while decreasing the pressure. The second jump happens at higher pressures, $P \sim 13$ and 21 bar for Run 1 and Run 2, respectively, and the jump in resonant frequency is

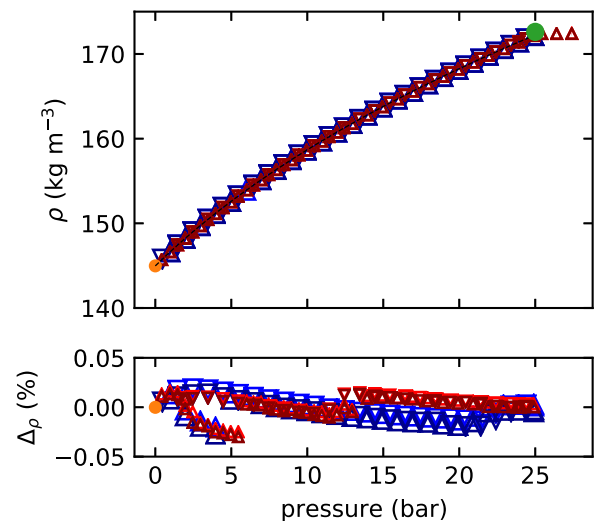


FIG. 7. Density of ^4He at 30 mK calculated using the Clausius-Mossotti relation (4) with polarizability $\alpha = 0.1234853 \text{ cm}^3$ of Ref. [23] and the deviation from the dielectric constant fit (12). Styles of points as in Fig. 6.

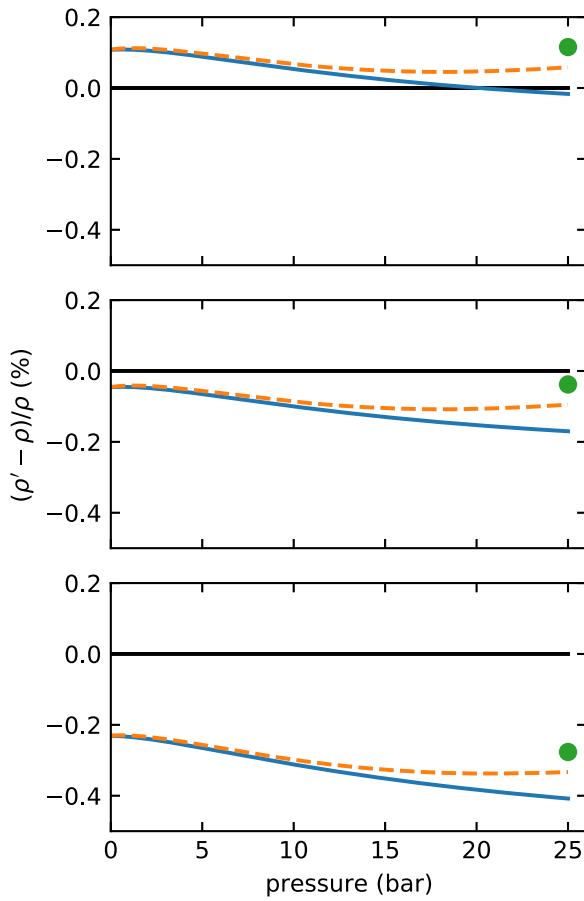


FIG. 8. The difference in measured pressure dependence of the density $(\rho' - \rho)/\rho$ where ρ' is either the data of Abraham *et al.* [31] (solid blue line) or Tanaka *et al.* [29] (dashed orange line) and ρ is the density obtained here. The single green point shows the freezing-point measurement of Berthold *et al.* [12]. The three panels show the effect of polarizability on ρ calculated from the dielectric constant (12) using the Clausius-Mossotti relation (4). Top panel, $\alpha = 0.1234853 \text{ cm}^3$ [23]; middle $\alpha = 0.123296 \text{ cm}^3$ [26]; and lower $\alpha = 0.123413 - 0.002376\rho \text{ cm}^3$ (where ρ is in g/cm^3) [41]. Using the polarizability of Ref. [38] results in low-pressure deviation reaching almost 1%.

observed both while increasing and decreasing the pressure. By taking multiple data sets we show that these jumps are repeatable at similar pressures.

We suspect that these jumps are caused by mechanical slipping—the cavity lid or pin coupler may shift at certain pressures, causing the resonant frequency to shift since the effective volume of the cavity changed. Berthold *et al.* [12] observed a similar effect, stating that the mechanical shock arising from the opening and closing of valves in their system can cause a frequency shift of up to 1 kHz in their cylindrical microwave cavity.

We calculate the density from μ with Clausius-Mossotti equations (4) using the polarizability determined through a helium-based dielectric constant gas thermometer near the triple point of water $\alpha = 0.1234853 \text{ cm}^3$ [23]. The resulting density and relative residuals are shown in Fig. 7. The residu-

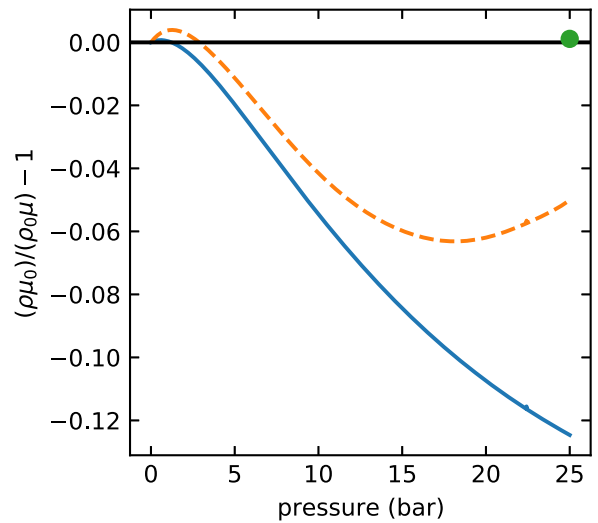


FIG. 9. The relative difference between density relative to the zero pressure ρ/ρ_0 obtained by Refs. [29,31] (same line styles as in Fig. 8) and Berthold *et al.* [12] (single green point) and our Clausius-Mossotti parameter μ relative to the zero pressure μ/μ_0 . For polarizability a density-independent constant, these relative parameters ought to be equal according to (4).

als are calculated with respect to the density calculated from the fit of ϵ in Eq. (12).

The calculated density crucially depends on the chosen value of polarizability. The pressure dependence of density is tabulated by Brooks and Donnelly [30] who derived values from the functional form reported by Abraham *et al.* [31]. Tanaka *et al.* [29] later made capacitive measurements of the helium density, producing their own functional form. The comparison of these two past experiments with the present data is shown in Fig. 8 using three different values of polarizability α . We see that, depending on the choice of polarizability, the typical deviations are quite significant and in the range 0.1%–0.5%. Note, however, that the apparent low-pressure agreement between Abraham *et al.* [31] and Tanaka *et al.* [29] is artificial since both of these experiments measured only relative change in density with respect to the zero-temperature, zero-pressure limit value ρ_0 . In both cases, $\rho_0 = 145.13 \text{ kg m}^{-3}$ was chosen, which was obtained by Kerr and Taylor [25] who measured changes in density with respect to a reference point near 1.2 K for which an error bar was not specified and then extrapolating a fit below approximately 1 K [25].

While the low-pressure value of ρ_0 has a fairly weak empirical basis and uncertainties in the polarizability complicate absolute comparisons, it is clear from Fig. 8 that pressure dependence differs among the experiments. This can also be seen in Fig. 9, which shows the relative deviation between ρ/ρ_0 measured by the authors of Refs. [29,31] and μ/μ_0 measured in our case (quantities with subscript 0 refer to values at zero pressure), which are independent of polarizability, if it is assumed to be pressure and density independent. In the present case, however, the largest uncertainties are likely due to cavity deformation which is not captured accurately enough using elastic compressibility. Another issue might arise in the neglected viscous flow through the heat exchanger in the cal-

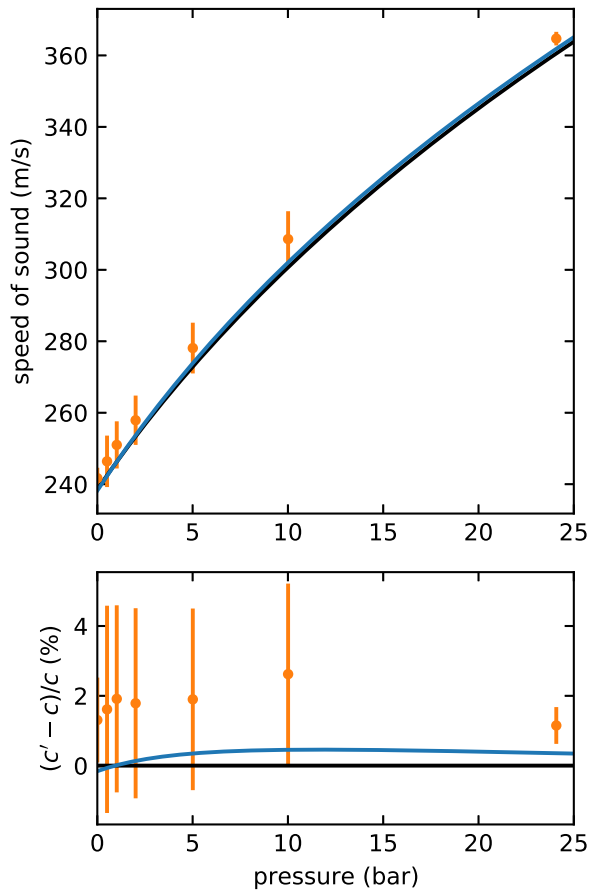


FIG. 10. (top) Speed of sound calculated from our pressure dependence of the dielectric constant using (12) and polarizability of Ref. [23] (black line), speed of sound from ultrasound pulse propagation [31] (blue line), and from inelastic neutron scattering [51] (orange points). (bottom) Relative deviation of the other datasets (c') from ours (c).

calculation of the fountain pressure correction of Eq. (9). These issues can be mitigated in future experiments, for example, using cryogenic valves and mechanically stronger cavity materials.

Finally, in Fig. 10(a) we show the speed of sound according to Eq. (5). Using the polynomial expression (12) and the Clausius-Mossotti equation (4) yields

$$c = \sqrt{\frac{4\pi\alpha}{3M_4}(A_1 + 2A_2\mu + 3A_3\mu^2)}, \quad (13)$$

where to obtain $c(P)$ the expression (12) is first inverted to obtain $\mu(P)$. In Fig. 10(b) we show the relative difference between the data obtained here and the speed of sound obtained using ultrasonic pulses by Abraham *et al.* [31] and inelastic neutron scattering by Godfrin *et al.* [51]. Apart from the low-pressure region, our data lie systematically below the ultrasound velocities. Since the data reported in Ref. [31]

have relative uncertainty of approximately 0.1% [due to the uncertainty of the zero-pressure limit value $c(0)$ and statistical uncertainty of the fit], this, again, most likely indicates that the deformation of the cavity is not fully accounted for by linear elastic compressibility.

VII. CONCLUSION

We presented measurements of the dielectric constant and density of superfluid ^4He in the zero-temperature limit for pressures up to 25 bar, showing that very high experimental accuracy is attainable under cryogenic conditions using a superconducting microwave cavity. Reviewing multiple past experiments, we find a systematic discrepancy between low-frequency and high-frequency measurements of the dielectric constant, which exceeds the expected frequency dependence of the polarizability [44]. For the pressure-dependent density, after careful consideration of dominant sources of systematic errors—a hydrostatic pressure head, fountain effect in the helium fill line, and the cavity compressibility—we find moderate discrepancies with respect to the values of density reported in the literature, which could be to a large extent attributed to the nonlinear deformation of the cavity geometry and rather uncertain value of the molecular polarizability of liquid ^4He . Finally, using the measured pressure dependence of density we calculate the speed of sound, which is found to be in good agreement, but systematically underestimating, the speed of sound obtained either by ultrasonic pulse propagation [31] or inelastic neutron scattering [51].

The uncertainty of polarizability in the high-density liquid is in stark contrast to the ^4He gas near the triple point of water, where experimental accuracy [23] and *ab initio* calculation of ^4He polarizability [44] advanced to the point where helium can be used for metrological purposes, such as the creation of a pressure standard. Such detailed, quantitative understanding of liquid helium under cryogenic conditions is equally desirable and would allow, for example, accurate calibration of cryogenic secondary pressure transducers. Thanks to high achievable quality factors of superconducting microwave cavities and the high purity of cryogenic liquid helium, extremely accurate measurements of dielectric properties of ^4He are possible, which presents an ideal test bed for future extensions of *ab initio* calculations. Finally, we note that if filled with ^3He , a similar system could be used as a highly accurate and sensitive primary thermometer at very low temperatures [52].

ACKNOWLEDGMENTS

This work was supported by the University of Alberta; the Natural Sciences and Engineering Research Council, Canada (Grants No. RGPIN-2016-04523, No. CREATE-2017-495446, and No. RGPIN-2022-03078); and the Alberta Quantum Major Innovation Fund.

[1] H. Padamsee, K. W. Shepard, and R. Sundelin, Physics and accelerator applications of RF superconductivity, *Annu. Rev. Nucl. Part. Sci.* **43**, 635 (1993).

[2] M. Reagor, W. Pfaff, C. Axline, R. W. Heeres, N. Ofek, K. Sliwa, E. Holland, C. Wang, J. Blumoff, K. Chou, M. J. Hatridge, L. Frunzio, M. H. Devoret, L. Jiang, and R. J.

- Schoelkopf, Quantum memory with millisecond coherence in circuit QED, *Phys. Rev. B* **94**, 014506 (2016).
- [3] C. Wang, Y. Y. Gao, P. Reinhold, R. W. Heeres, N. Ofek, K. Chou, C. Axline, M. Reagor, J. Blumoff, K. M. Sliwa, L. Frunzio, S. M. Girvin, L. Jiang, M. Mirrahimi, M. H. Devoret, and R. J. Schoelkopf, A Schrödinger cat living in two boxes, *Science* **352**, 1087 (2016).
- [4] M. Reagor, H. Paik, G. Catelani, L. Sun, C. Axline, E. Holland, I. M. Pop, N. A. Masluk, T. Brecht, L. Frunzio, M. H. Devoret, L. Glazman, and R. J. Schoelkopf, Reaching 10 ms single photon lifetimes for superconducting aluminum cavities, *Appl. Phys. Lett.* **102**, 192604 (2013).
- [5] M. Kudra, J. Biznářová, A. Fadavi Roudsari, J. J. Burnett, D. Niepce, S. Gasparinetti, B. Wickman, and P. Delsing, High quality three-dimensional aluminum microwave cavities, *Appl. Phys. Lett.* **117**, 070601 (2020).
- [6] J. H. Béjanin, C. T. Earnest, A. S. Sharafeldin, and M. Mariantoni, Interacting defects generate stochastic fluctuations in superconducting qubits, *Phys. Rev. B* **104**, 094106 (2021).
- [7] C. Müller, J. H. Cole, and J. Lisenfeld, Towards understanding two-level-systems in amorphous solids: Insights from quantum circuits, *Rep. Prog. Phys.* **82**, 124501 (2019).
- [8] J. M. Martinis, K. B. Cooper, R. McDermott, M. Steffen, M. Ansmann, K. D. Osborn, K. Cicak, S. Oh, D. P. Pappas, R. W. Simmonds, and C. C. Yu, Decoherence in Josephson Qubits from Dielectric Loss, *Phys. Rev. Lett.* **95**, 210503 (2005).
- [9] A. Tretiakov, C. A. Potts, T. S. Lee, M. J. Thiessen, J. P. Davis, and L. J. LeBlanc, Atomic microwave-to-optical signal transduction via magnetic-field coupling in a resonant microwave cavity, *Appl. Phys. Lett.* **116**, 164101 (2020).
- [10] M. Ruether, C. A. Potts, J. P. Davis, and L. J. LeBlanc, Polymer-loaded three dimensional microwave cavities for hybrid quantum systems, *J. Phys. Commun.* **5**, 121001 (2021).
- [11] H. N. Hanson, J. E. Berthold, G. M. Seidel, and H. J. Maris, Density of liquid ^4He at freezing and entropy of solid ^4He at low temperatures, *Phys. Rev. B* **14**, 1911 (1976).
- [12] J. E. Berthold, H. N. Hanson, H. J. Maris, and G. M. Seidel, Investigation of the phonon dispersion relation in liquid ^4He by thermal-expansion measurements, *Phys. Rev. B* **14**, 1902 (1976).
- [13] F. Souris, H. Christiani, and J. P. Davis, Tuning a 3D microwave cavity via superfluid helium at millikelvin temperatures, *Appl. Phys. Lett.* **111**, 172601 (2017).
- [14] J. R. Lane, D. Tan, N. R. Beysengulov, K. Nasyedkin, E. Brook, L. Zhang, T. Stefanski, H. Byeon, K. W. Murch, and J. Pollanen, Integrating superfluids with superconducting qubit systems, *Phys. Rev. A* **101**, 012336 (2020).
- [15] L. A. De Lorenzo and K. C. Schwab, Superfluid optomechanics: Coupling of a superfluid to a superconducting condensate, *New J. Phys.* **16**, 113020 (2014).
- [16] S. Singh, L. A. Lorenzo, I. Pikovski, and K. C. Schwab, Detecting continuous gravitational waves with superfluid ^4He , *New J. Phys.* **19**, 073023 (2017).
- [17] A. V. Smorodin, A. S. Rybalko, and D. Konstantinov, Measurements of the complex permittivity of liquid helium-4 in the millimeter wave range by a whispering gallery mode resonator, *J. Low Temp. Phys.* **187**, 361 (2017).
- [18] V. Vadakkumbatt, M. Hirschel, J. Manley, T. J. Clark, S. Singh, and J. P. Davis, Prototype superfluid gravitational wave detector, *Phys. Rev. D* **104**, 082001 (2021).
- [19] J. Manley, D. J. Wilson, R. Stump, D. Grin, and S. Singh, Searching for Scalar Dark Matter with Compact Mechanical Resonators, *Phys. Rev. Lett.* **124**, 151301 (2020).
- [20] A. A. Zadorozhko, Y. P. Monarkha, and D. Konstantinov, Circular-Polarization-Dependent Study of Microwave-Induced Conductivity Oscillations in a Two-Dimensional Electron Gas on Liquid Helium, *Phys. Rev. Lett.* **120**, 046802 (2018).
- [21] J. Pollanen, N. Beysengulov, and D. Rees, U.S. Patent No. 10,892,398.
- [22] P. M. C. Rourke, Perspective on the refractive-index gas metrology data landscape, *J. Phys. Chem. Ref. Data* **50**, 033104 (2021).
- [23] C. Gaiser and B. Fellmuth, Polarizability of Helium, Neon, and Argon: New Perspectives for Gas Metrology, *Phys. Rev. Lett.* **120**, 123203 (2018).
- [24] C. J. Grebenkemper and J. P. Hagen, The dielectric constant of liquid helium, *Phys. Rev.* **80**, 89 (1950).
- [25] E. C. Kerr and R. D. Taylor, The molar volume and expansion coefficient of liquid ^4He , *Ann. Phys. (NY)* **26**, 292 (1964).
- [26] R. F. Harris-Lowe and K. A. Smee, Thermal expansion of liquid helium II, *Phys. Rev. A* **2**, 158 (1970).
- [27] E. M. Ganapolskii, A. V. Golik, and A. P. Korolyuk, Observation of an electromagnetic absorption peak in the millimeter wave range in liquid helium at the superfluid λ transition, *Phys. Rev. B* **51**, 11962 (1995).
- [28] J. J. Niemela and R. J. Donnelly, Density and thermal expansion coefficient of liquid helium-4 from measurements of the dielectric constant, *J. Low Temp. Phys.* **98**, 1 (1995).
- [29] E. Tanaka, K. Hatakeyama, S. Noma, and T. Satoh, Molar volume of pure liquid ^4He : Dependence on temperature (50–1000 mK) and pressure (0–1.57 MPa), *Cryogenics* **40**, 365 (2000).
- [30] J. S. Brooks and R. J. Donnelly, The calculated thermodynamic properties of superfluid helium-4, *J. Phys. Chem. Ref. Data* **6**, 51 (1977).
- [31] B. M. Abraham, Y. Eckstein, J. B. Ketterson, M. Kuchmir, and P. R. Roach, Velocity of sound density, and gruneisen constant in liquid ^4He , *Phys. Rev. A* **2**, 550 (1970).
- [32] D. M. Pozar, *Microwave Engineering*, 4th ed., (Wiley, New York, 2011).
- [33] M. J. Reagor, Superconducting Cavities for Circuit Quantum Electrodynamics, Ph.D. thesis, Yale (2015).
- [34] The polarizability volume per mole α is related to the molecular polarizability (per mole) $p = 4\pi\epsilon_0\alpha$. In the dielectric constant gas thermometry literature (e.g., Ref. [23]) the common definition of polarizability is $A_\epsilon = 4\pi\alpha/3$.
- [35] M. A. Allen, Z. D. Farkas, H. A. Hogg, E. W. Hoyt, and P. B. Wilson, Superconducting niobium cavity measurements at SLAC, *IEEE Trans. Nucl. Sci.* **18**, 168 (1971).
- [36] S. Probst, F. B. Song, P. A. Bushev, A. V. Ustinov, and M. Weides, Efficient and robust analysis of complex scattering data under noise in microwave resonators, *Rev. Sci. Instrum.* **86**, 024706 (2015).
- [37] D. R. Tilley and J. Tilley, *Superfluidity and Superconductivity*, 3rd ed., (IOP Publishing, Bristol, England, 1990).
- [38] V. D. Arp, R. D. McCarty, and D. G. Friend, Thermophysical Properties of Helium-4 from 0.8 to 1500 K with Pressures to 2000 MPa, Technical Note No. 1334 (NIST TN) (1998).
- [39] J. Ekin, *Experimental Techniques for Low-Temperature Measurements: Cryostat Design, Material Properties, and*

- Superconductor Critical-Current Testing* (Oxford University Press, Oxford, 2006).
- [40] S. W. V. Sciver, *Helium Cryogenics*, 2nd ed., International Cryogenics Monograph Series, (Springer, New York, 2012).
- [41] E. C. Kerr and R. H. Sherman, The molar polarizability of ^3He at low temperatures and its density dependence, *J. Low Temp. Phys.* **3**, 451 (1970).
- [42] H. A. Kierstead, Dielectric constant and molar volume of saturated liquid ^3He and ^4He , *J. Low Temp. Phys.* **23**, 791 (1976).
- [43] M. Chan, M. Ryschkewitsch, and H. Meyer, The dielectric constant in liquid and solid ^4He , *J. Low Temp. Phys.* **26**, 211 (1977).
- [44] K. Piszczatowski, M. Puchalski, J. Komasa, B. Jezierski, and K. Szalewicz, Frequency-Dependent Polarizability of Helium Including Relativistic Effects with Nuclear Recoil Terms, *Phys. Rev. Lett.* **114**, 173004 (2015).
- [45] A. D. Buckingham and J. A. Pople, The dielectric constant of an imperfect non-polar gas, *Trans. Faraday Soc.* **51**, 1029 (1955).
- [46] T. L. Hill, Theory of the dielectric constant of imperfect gases and dilute solutions, *J. Chem. Phys.* **28**, 61 (1958).
- [47] H.-Y. Kim, J. O. Sofo, D. Velegol, M. W. Cole, and G. Mukhopadhyay, Static polarizabilities of dielectric nanoclusters, *Phys. Rev. A* **72**, 053201 (2005).
- [48] C. Gaiser, B. Fellmuth, and N. Haft, Primary dielectric-constant gas thermometry in the range from 2.4 K to 26 K at PTB, *Int J Thermophys* **29**, 18 (2008).
- [49] P. J. Brown and W. A. Fuller, *Statistical Analysis of Measurement Error Models and Applications: Proceedings of the AMS-IMS-SIAM Joint Summer Research Conference Held June 10-16, 1989, with Support from the National Science Foundation and the U.S. Army Research Office* (American Mathematical Society, Washington, D.C., 1990).
- [50] B. Efron, Nonparametric estimates of standard error: The jackknife, the bootstrap and other methods, *Biometrika* **68**, 589 (1981).
- [51] H. Godfrin, K. Beauvois, A. Sultan, E. Krotscheck, J. Dawidowski, B. Fåk, and J. Ollivier, Dispersion relation of Landau elementary excitations and thermodynamic properties of superfluid ^4He , *Phys. Rev. B* **103**, 104516 (2021).
- [52] D. S. Greywall and P. A. Busch, ^3He -melting-curve thermometry, *J. Low Temp. Phys.* **46**, 451 (1982).